Astronomy & Astrophysics manuscript no. Bonomo˙KOI135b˙203b˙204b
October 26, 2011
© ESO 2011

arXiv:1110.5462v1 [astro-ph.EP] 25 Oct 2011

SOPHIE velocimetry of *Kepler* transit candidates⋆

V. The three hot Jupiters KOI-135b, KOI-204b and KOI-203b (alias Kepler-17b)

A. S. Bonomo[1], G. Hébrard[2,3], A. Santerne[1,3], N. C. Santos[4,5], M. Deleuil[1], J. Almenara[1], F. Bouchy[2,3], R. F. Díaz[2,3], C. Moutou[1], and M. Vanhuysse[6].

[1] Laboratoire d'Astrophysique de Marseille, Université Aix-Marseille & CNRS, 38 rue Frédéric Joliot-Curie, F-13388 Marseille Cedex 13, France
[2] Institut d'Astrophysique de Paris, UMR7095 CNRS, Université Pierre & Marie Curie, 98bis boulevard Arago, 75014 Paris, France
[3] Observatoire de Haute-Provence, Université Aix-Marseille & CNRS, F-04870 St. Michel l'Observatoire, France
[4] Centro de Astrofísica, Universidade do Porto, Rua das Estrelas, 4150-762 Porto, Portugal
[5] Departamento de Física e Astronomia, Faculdade de Ciências, Universidade do Porto, Portugal
[6] Oversky, 47 Alle des Palanques, 33127, Saint Jean d'Illac, France

Received ?? / Accepted ??

ABSTRACT

We report the discovery of two new transiting hot Jupiters, KOI-135b and KOI-204b, that were previously identified as planetary candidates by Borucki et al. 2011, and, independently of the Kepler team, confirm the planetary nature of Kepler-17b, recently announced by Désert et al. 2011. Radial-velocity measurements, taken with the SOPHIE spectrograph at the Observatoire de Haute-Provence (France), and Kepler photometry (Q1 and Q2 data) were used to derive the orbital, stellar and planetary parameters. KOI-135b and KOI-204b orbit their parent stars in ∼ 3.02 and 3.25 days, respectively. They have approximately the same radius, R_p = 1.20 ± 0.06 R_{Jup} and 1.24 ± 0.07 R_{Jup}, but different masses M_p = 3.23 ± 0.19 M_{Jup} and 1.02 ± 0.07 M_{Jup}. As a consequence, their bulk densities differ by a factor of four, $\rho_p = 2.33 \pm 0.36\,g\,cm^{-3}$ (KOI-135b) and $0.65 \pm 0.12\,g\,cm^{-3}$ (KOI-204b), meaning that their interior structures are different. All the three planets orbit metal-rich stars with [Fe/H] ∼ 0.3 dex. Our SOPHIE spectra of Kepler-17b, used both to measure the radial-velocity variations and determine the atmospheric parameters of the host star, allow us to refine the characterisation of the planetary system. In particular we found the radial-velocity semi-amplitude and the stellar mass to be respectively slightly smaller and larger than Désert et al. These two quantities, however, compensate and lead to a planetary mass fully consistent with Désert et al. : our analysis gives M_p = 2.47 ± 0.10 M_{Jup} and R_p = 1.33 ± 0.04 R_{Jup}. We found evidence for a younger age of this planetary system, t < 1.8 Gyr, which is supported by both evolutionary tracks and gyrochronology. Finally, we confirm the detection of the optical secondary eclipse by Désert et al. and found also the brightness phase variation with the Q1 and Q2 Kepler data. The latter indicates a low redistribution of stellar heat to the night side (< 16% at 1-σ), if the optical planetary occultation comes entirely from thermal flux. The geometric albedo is A_g < 0.12 (1-σ).

Key words. planetary systems – stars: fundamental parameters – techniques: photometric – techniques: spectroscopic – techniques: radial velocities.

1. Introduction

Since two years and a half, the Kepler space telescope is monitoring the optical flux of about 156,000 stars with 9 < V < 16 in the Cygnus constellation to search for transiting planets (e.g., Borucki et al. 2006). More than 1200 planetary candidates have been announced by Borucki et al. (2011) in February 2011. However, all of them cannot be followed up by the Kepler team as this would require a huge amount of telescope time. Since the Kepler team publicly announced all the planetary candidates they found, this allows also other groups to carry out spectroscopic observations of their targets.

The SOPHIE spectrograph (Bouchy et al. 2009), mounted on the 1.93 m telescope at the Observatoire de Haute Provence (France), has been performing very well to assess the nature of CoRoT planetary candidates and derive the orbital parameters of many CoRoT planets (e.g., Deleuil et al. 2011). Therefore, about one year and a half ago, we started the spectroscopic follow-up of Kepler candidates with Jupiter and Saturn sizes, around stars with K_p[1]< 14.7. So far, this follow-up campaign led to several interesting discoveries: one new hot Jupiter orbiting an evolved star, KOI-428b (Santerne et al. 2010); KOI-423b, a 18 M_{Jup} companion orbiting a subgiant F7IV star, that could be either a low-mass brown dwarf or an extremely massive planet (Bouchy et al. 2011); and the hot Jupiter KOI-196b for which we detected the optical secondary eclipse and phase variations (Santerne et al. 2011). Moreover, this follow-up campaign is revealing the rate of Kepler Jupiter-size planetary candidates that are actually false positives, to be compared with the ∼ 8% upper limit predicted by Morton & Johnson (2011) (Santerne et al., in preparation).

In the present paper, we announce the discovery of two new hot Jupiters with an orbital period of ∼ 3 days, namely KOI-135b and KOI-204b. Orbital and planetary parameters for these two planets were derived by performing a simultaneous modelling

Send offprint requests to:
e-mail: aldo.bonomo@oamp.fr

⋆ Based on observations made with SOPHIE on the 1.93-m telescope at Observatoire de Haute-Provence (CNRS), France

[1] Kepler magnitude

of Kepler photometry and SOPHIE radial-velocity observations. Moreover, independently from the Kepler team, we confirm the planetary nature of Kepler-17b, a hot Jupiter around an active solar-like star, recently announced by Désert et al. (2011). Our new SOPHIE spectra, used both to measure the radial-velocity variations and characterise the host star, allow us to improve the parameters of this planetary system. Besides that, we detected the optical phase variations of Kepler-17b, i.e. the variation in brightness as the dayside of the planet rotates into and out of view, not reported previously, and discuss its possible implications for the planet atmosphere.

2. KOI-135

2.1. Kepler observations

KOI-135 is a K_p = 14.0 star and was observed by Kepler with a temporal sampling of 29.4 min (Long Cadence data) for 122.2 days: from May, 13 to June, 15, 2009 during the first 33.5-day segment of science operations (Q1), and from June, 20 to September, 16 of the same year, during the second quarter (Q2) data lasting 88.7 days. Its coordinates, magnitudes and IDs are listed in Table 1. The raw Kepler light curve, publicly available at the MAST archive[2], contains 5722 validated photometric measurements. From these data points we subtracted the flux excess due to background stars contaminating the photometric mask, as estimated by the Kepler team: 2.4% for the Q1 and 3.1% for the Q2 data [3]. Long-term trends of clear instrumental origin and the steep variations after the two safe modes (Jenkins et al. 2010) were then removed. The so-treated light curve is shown in Fig. 1. It exhibits thirty-nine transits with a period of 3.02 days, a depth of 0.8% and a duration of $\sim$ 3 hours. The standard deviation of the light curve, computed in a robust way after removing low frequency variations with a sliding median filter, is 180 ppm, which is compatible with the median of the errors of the single photometric measurements, i.e. 160 ppm.

Stellar variability due to the rotational modulation of active regions on the stellar photosphere is clearly visible in the light curve (Fig. 1). Its peak-to-peak amplitude is about 0.5%. After removing transits, we performed a periodogram analysis of the light curve and computed the autocorrelation function in order to estimate the stellar rotation period. The two methods give very consistent results: $P_{*,\mathrm{rot}} = 12.9 \pm 0.7$ days.

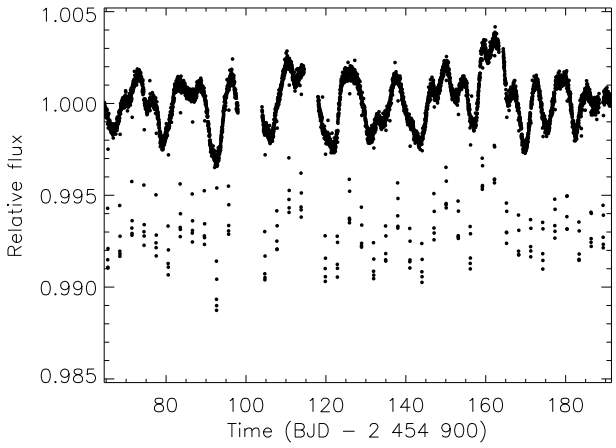

Fig. 1. The Kepler light curve of KOI-135 with a temporal sampling of 29.4 min showing 39 transits and flux variations due to stellar activity with a peak-to-peak amplitude of $\sim$ 0.5%. Long-term trends and the steep variations after the safe modes were removed.

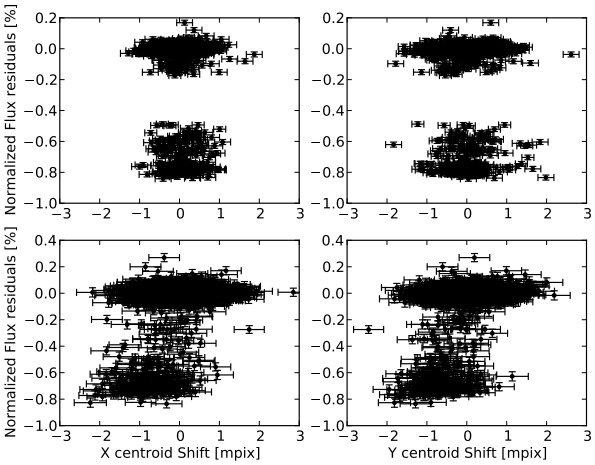

Fig. 2. Rain plots showing X (left panels) and Y (right panels) shifts of the centroid as a function of the normalized flux measured during the transits of KOI-135b (upper panels) and KOI-204b (lower panels).

2.2. Centroid analysis

In order to reject the scenario of a background eclipsing binary located within the Kepler photometric mask, that might mimic the observed transits, the centroid timeseries was analysed (Batalha et al. 2010). KOI-135 does not show any significant centroid shift during the transit up to 0.07 mpixel (Fig. 2).

2.3. Ground-based follow-up

2.3.1. Radial-velocity observations

Eight spectra of KOI-135 were secured during the summer 2011 with the SOPHIE spectrograph. They were acquired in High-Efficiency mode (resolution power R = 39 000 at 5500 Å) and slow-mode for the reading of the detector. The first aperture fiber was put on the target whereas the second 2' away on the sky in order to evaluate the background. The spectra extraction was performed using the SOPHIE pipeline. Following the techniques described by Baranne et al. (1996) and Pepe et al. (2002), the radial velocities were measured from a weighted cross-correlation of the spectra with a numerical mask. We used a standard G2 mask that includes more than 3500 lines. The resulting cross-correlation functions (CCFs) were fitted by Gaussians to get the radial velocities and the associated photon-noise errors. The full width at half maximum of those Gaussians is 11.6 ± 0.1 km s^{-1}, and its contrast is 24 ± 2 % of the continuum. We only used the spectral orders 12 to 38 in the cross-correlation to reduce the dispersion of the measurements produced by noisy spectral orders. Moonlight contamination was tenuous in the spectra and required a correction only for two over the eight spectra, following the method described in Pollacco et al. (2008) and

[2] http://archive.stsci.edu/kepler/data_search/search.php
[3] http://archive.stsci.edu/kepler/kepler_fov/search.php

Table 1. IDs, coordinates, and magnitudes of the planet-hosting stars KOI-135, 204, and 203.

Kepler Object of Interest	KOI-135	KOI-204	KOI-203
Kepler ID	9818381	9305831	10619192
USNO-A2 ID	1350-10117895	1350-11449251	1350-11245067
2MASS ID	19005780+4640057	20002456+4545437	19533486+4748540
Coordinates			
RA (J2000)	19:00:57.82	20:0:24.55	19:53:34.87
Dec (J2000)	46:40:5.88	45:45:43.56	47:48:54.0
Magnitudes			
Filter			
K_p [a]	13.96	14.68	14.14
J [b]	12.86 (0.02)	13.34 (0.03)	12.99 (0.02)
H [b]	12.60 (0.02)	12.97 (0.02)	12.67 (0.02)
K [b]	12.55 (0.03)	12.89 (0.03)	12.58 (0.02)

a: Kepler magnitude from MAST Archive; *b*: from 2MASS catalogue.

Hébrard et al. (2008). It introduced modest corrections (7 and 20 $\mathrm{m\,s^{-1}}$ for the two spectra).

The log of the observations and the radial-velocity measurements are reported in Table 2. Radial-velocity precision ranges between 12 and 29 $\mathrm{m\,s^{-1}}$ depending on the exposure time and weather conditions. Table 2 also lists the bisector spans that we measured on the cross-correlation functions in order to quantify the possible shape variations of the spectral lines. The error bars on the bisector spans were assumed to be twice those of the corresponding radial velocity.

The measurements are displayed in Fig. 3, left panel, together with their circular Keplerian fit obtained from the global photometry and radial-velocity best fit (Sect. 2.4). The radial velocities present a semi-amplitude $K = 375 \pm 13\ \mathrm{m\,s^{-1}}$, in phase with the Kepler ephemeris. The standard deviation of the residuals to the fit is $\sigma_{O-C} = 15.9\ \mathrm{m\,s^{-1}}$. The reduced χ^2 is 1.0 for the eight radial velocities used in the fit. We do not detect any drift over the 55-day span of the radial velocity.

SOPHIE radial velocities obtained with different stellar masks (F0, K0, or K5) produce variations with the same amplitude as for the G2 mask and, thus, there is no indication for blend scenarios implying stars of different spectral types. Similarly, the CCF bisector spans show neither variations nor trend as a function of radial velocity (Fig. 4, left panel). This reinforces the conclusion that the radial-velocity variations are caused by a planetary companion and not by changes in the spectral line profile due to blends.

2.3.2. Stellar characterisation

Stellar parameters and iron abundances were derived in LTE, using a grid of plane-parallel, ATLAS9 model atmospheres (Kurucz 1993) and the 2002 version of the radiative transfer code MOOG (Sneden 1973). The methodology used is described in detail in Santos et al. (2004), Sousa et al. (2008) and references therein. The full spectroscopic analysis is based on the EWs of a set of 49 Fe I and 13 Fe II weak lines, by imposing ionization and excitation equilibrium, as well as a zero slope between the abundances given by individual lines and their equivalent width. The errors in the stellar parameters were derived using the same methodology as described in Gonzalez (1998).

The total S/N of the SOPHIE spectra used for this analysis (co-added from several individual spectra used to derive radial-velocities) is 36 per pixel (0.02 Å) at 5500 Å. We subtracted the background sky light on the science spectra using the second SOPHIE aperture positioned on the sky. The EWs were carefully measured one by one using the IRAF splot routine.

For FGK dwarfs, the stellar parameters obtained using this methodology were shown to be compatible with other estimates in the literature. In particular, the derived effective temperatures are very close to the ones obtained using recent applications of the infra-red flux method (Casagrande et al. 2006). For a recent comparison we refer to Sousa et al. (2011).

The atmospheric parameters for the host star KOI-135, determined with the described procedure, are $T_{\rm eff} = 6041 \pm 143$ K, $\log g = 4.64 \pm 0.13$, and metallicity [Fe/H] $= 0.33 \pm 0.11$. No detectable emission was found in the cores of Ca II H & K lines. The $V \sin i_*$ of $5.5 \pm 1.5\ \mathrm{km\,s^{-1}}$ is in agreement with the rotation period determined from the light curve, assuming a stellar inclination of $i_* \sim 90$ degrees.

2.4. System parameters

To derive the orbital and planetary parameters, a simultaneous fit of Kepler photometry and SOPHIE radial velocity measurements was performed. All the transits were normalised by fitting a parabola to the 11 hours intervals of the light curve before the ingress and after the egress of each transit. We discarded two of the thirty-nine available transits, specifically those occurring at 2455056.139, and 2455089.404 BJD. Indeed, the out-of-transit intervals around these epochs were not sufficiently wide to correctly normalise the transits.

The nine free parameters of our global best fit are the orbital period P, the transit epoch $T_{\rm tr}$; the transit duration T_{14}; the ratio of the planet to stellar radii $R_{\rm p}/R_*$; the inclination i between the orbital plane and the plane of the sky; the Lagrangian orbital elements $h = e\ \sin\omega$ and $k = e\ \cos\omega$, where e is the eccentricity and ω the argument of the periastron; the radial-velocity semi-amplitude K; and the systemic radial velocity γ_{rel}. The two non-linear limb-darkening coefficients $u_+ = u_a + u_b$ and $u_- = u_{\rm a} - u_{\rm b}$ [4] were fixed in our analysis. They can not be let as free parameters as the orbital period is almost an integer multiple of the long-cadence sampling $\delta t = 29.42$ min, $P = 147.986 \cdot \delta t$, which

[4] $u_{\rm a}$ and $u_{\rm b}$ are the coefficients of the limb-darkening quadratic law: $I(\mu)/I(1) = 1 - u_{\rm a}(1-\mu) - u_{\rm b}(1-\mu)^2$, where $I(1)$ is the specific intensity at the centre of the disc and $\mu = \cos\gamma$, γ being the angle between the surface normal and the line of sight

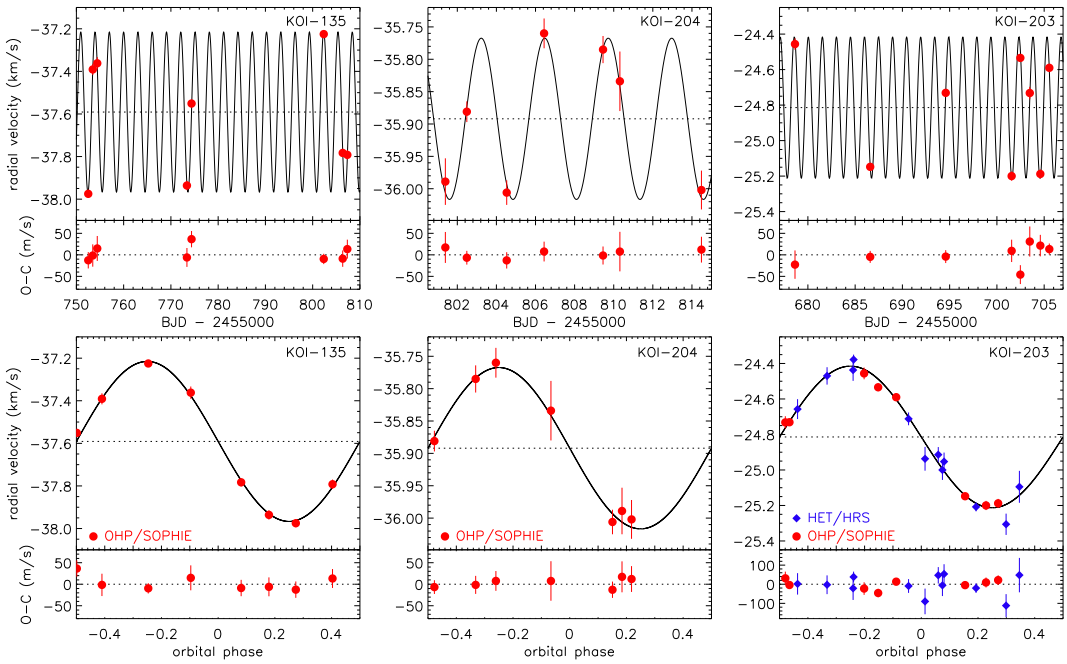

Fig. 3. *Upper panel:* Radial-velocity measurements of the three targets with 1-σ error bars as a function of time together with their Keplerian fit (*top*) and residuals of the fit. *Lower panel:* Same as above but as a function of the orbital phase.

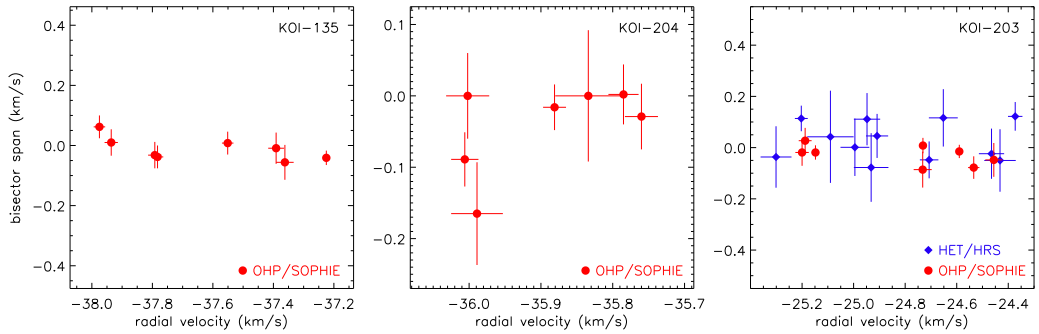

Fig. 4. Bisector span as a function of the radial velocities with 1-σ error bars for the three targets. The ranges have the same extents in the *x*- and *y*-axes.

implies that the transit ingress and egress are not well sampled (see Fig. 5). The adopted limb-darkening coefficients u_a and u_b for the Kepler bandpass were taken from Sing (2010) Tables[5], after linearly interpolating at the $T_{\rm eff}$, $\log g$ and metallicity of the star: $u_a = 0.375 \pm 0.026$ and $u_b = 0.277 \pm 0.015$, which give $u_+ = 0.652 \pm 0.030$ and $u_- = 0.098 \pm 0.030$.

The transit fitting was carried out using the model of Giménez (2006, 2009) and a denser temporal sampling $\delta t_{\rm model} = \delta t/5$, as suggested by Kipping & Bakos (2011) to overcome the problem of the coarse Kepler sampling (see also Kipping 2010). The χ^2 of each trial model is then computed by binning the model samples at the Kepler sampling rate δt. The search for the best solution of our combined fit was performed by using the algorithm AMOEBA (Press et al. 1992) and changing the initial values of the parameters with a Monte-Carlo method to avoid the solution to get stuck into a local minimum. The 1-σ errors of the system parameters were estimated through a bootstrap procedure consisting in shifting the photometric residuals and, at the same time, shuffling the radial velocity ones. During the bootstrap procedure, the limb-darkening coefficients were let vary within their error bars related to the uncertainties of the atmospheric parameters (see Sect. 6.3 in Bouchy et al. 2011 for more details).

The system parameters and their 1-σ errors are listed in Table 3. The radial-velocity measurements taken with the SOPHIE spectrograph and the solution of the Keplerian fit derived from our combined fit are shown in Fig. 3. Figure 5 displays the phase-folded transit light curve of KOI-135b and, superposed, the transit model.

As stated before, the transits of KOI-135b are not well sampled because the orbital period is almost an integer multiple of the Kepler long-cadence rate. For this reason we performed some additional best fits by considering also transit models with a sampling denser than $\delta t/5$, i.e. $\delta t_{\rm model} = \delta t/9$ and $\delta t/15$. We always found a solution compatible with that reported in Table 3 within 1-σ and, thus, conclude that $\delta t_{\rm model} = \delta t/5$ gives an accurate enough solution for the transit parameters.

[5] http://vega.lpl.arizona.edu/singd/David_Sing/Limb_Darkening.html

Table 2. SOPHIE radial-velocity measurements.

BJD_{UTC} -2 400 000	RV (km s^{-1})	$\pm1\,\sigma$ (km s^{-1})	Bis. span (km s^{-1})	exp. time (sec)	S/N p. pix. (at 550 nm)	Target
55752.5089	-37.975	0.019	0.062	1562	19.5	KOI-135
55753.4652†	-37.391	0.026	-0.009	3600	16.0	KOI-135
55754.4127†	-37.362	0.029	-0.056	3600	14.2	KOI-135
55773.3908	-37.936	0.022	0.010	3600	17.5	KOI-135
55774.3658	-37.551	0.019	0.008	3600	18.4	KOI-135
55802.3448	-37.225	0.012	-0.041	3600	26.3	KOI-135
55806.3595	-37.783	0.019	-0.038	2703	19.0	KOI-135
55807.3341	-37.792	0.022	-0.032	3600	17.7	KOI-135
55801.3890	-35.989	0.036	-0.165	3600	10.9	KOI-204
55802.4872	-35.881	0.016	-0.016	3600	18.3	KOI-204
55804.5266	-36.006	0.019	-0.089	3101	16.0	KOI-204
55806.4383	-35.760	0.023	-0.029	2249	14.1	KOI-204
55809.4533	-35.785	0.021	0.002	3600	14.9	KOI-204
55810.3153†	-35.834	0.046	-0.000	2543	10.0	KOI-204
55814.4852	-36.002	0.030	0.000	3600	17.5	KOI-204
55678.6344†	-24.456	0.033	-0.048	1562	12.3	KOI-203
55686.5921	-25.148	0.014	-0.019	3600	22.8	KOI-203
55694.5860	-24.731	0.015	0.008	3600	22.2	KOI-203
55701.5588†	-25.200	0.026	-0.019	3600	16.9	KOI-203
55702.4793†	-24.534	0.022	-0.078	3600	18.2	KOI-203
55703.4786†	-24.732	0.035	-0.086	3600	13.2	KOI-203
55704.5938†	-25.188	0.025	0.027	2703	17.8	KOI-203
55705.5453†	-24.590	0.013	-0.015	3600	24.5	KOI-203

†: measurements corrected from Moonlight pollution.

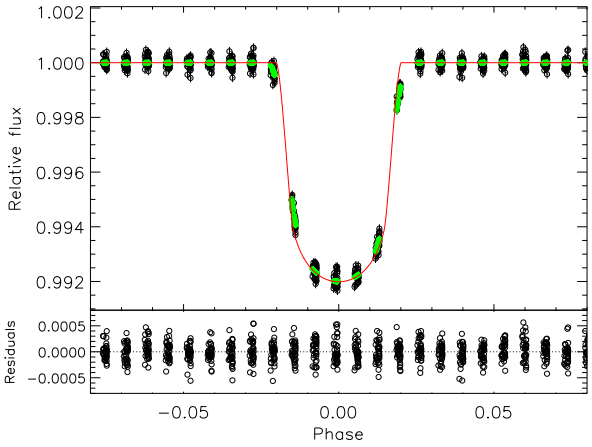

Fig. 5. *Top panel*: Unbinned phase-folded transit light curve of KOI-135 (black circles). The red solid line shows the transit model oversampled five times denser than the Kepler sampling rate. The green diamonds indicate the model samples binned to match the Kepler sampling. *Bottom panel*: the residuals from the best-fit model.

2.5. Stellar and planetary parameters

The stellar density derived from the transit fitting and the STAREVOL evolutionary tracks (Palacios, private communication; Siess 2006) for the effective temperature and metallicity of KOI-135 point to a star with mass $M_\star = 1.32 \pm 0.09$ $M_\odot$ and radius $R_\star = 1.42 \pm 0.07$ $R_\odot$. The quoted errors on stellar parameters take into account also the uncertainties inherent in stellar models, which are typically 3% and 5% for the stellar radius and mass, respectively (Southworth 2011; see also Sect. 4 in Désert et al. 2011). The latter were quadratically added to the statistical errors on $M_\star$ and $R_\star$ related to the stellar density from the transit best fit.

We point out that the surface gravity deduced from the aforementioned stellar parameters, $\log g = 4.26 \pm 0.05$, is compatible with the spectroscopic $\log g$ at 2.7 σ. However, it is well known that the surface gravity derived from a spectral analysis is the most uncertain atmospheric parameter and, thus, such an apparent discrepancy must not be of great concern. In other words, our error bars on the spectroscopic $\log g$ are likely underestimated. Fixing the $\log g$ to the photometric determination and performing again the spectral analysis letting only the $T_{\rm eff}$ and metallicity vary, changes only slightly the solution reported in Sect. 2.3.2, well within the 1-σ uncertainties.

According to the determined stellar parameters, the mass and radius of the hot Jupiter KOI-135b are $M_{\rm p} = 3.23 \pm 0.19$ $M_{\rm Jup}$ and $R_{\rm p} = 1.20 \pm 0.06$ $R_{\rm Jup}$. The corresponding planet density is 2.33 ± 0.36 g cm^{-3}. The STAREVOL evolutionary tracks indicate that the age of the star, and thus of the planetary system KOI-135, is $2.8^{+1.0}_{-0.8}$ Gyr. This age is in good agreement with the estimate given by gyrochronology (Barnes 2007), i.e. 1.6 ± 0.7 Gyr [6]. We point out that the agreement is even better when considering the "modified gyrochronology" by Lanza (2010), which takes the influence of the planet on the evolution of stellar angular momentum into account and gives 3.0 ± 1.3 Gyr.

3. KOI-204

3.1. Kepler observations

The target KOI-204 is a faint star with Kepler magnitude $K_{\rm p}$ = 14.7. Its coordinates, magnitudes and IDs are listed in Table 1.

[6] using B-V=0.58 ± 0.04 estimated from Eq. 3 in Sekiguchi & Fukugita (2000)

Table 3. KOI-135 and 204: planet and star parameters.

Fitted system parameters	KOI-135	KOI-204
Planet orbital period P [days]	3.024095 ± 0.000021	3.246740 ± 0.000018
Planetary transit epoch $T_{\rm tr}$ [BJD-2400000]	54965.4159 ± 0.0006	54966.3781 ± 0.0004
Planetary transit duration T_{14} [h]	2.926 ± 0.019	3.218 ± 0.043
Radius ratio $R_{\rm p}/R_*$	$0.0868^{+0.0006}_{-0.0007}$	0.0844 ± 0.0011
Inclination i [deg]	$84.35^{+0.47}_{-0.40}$	$83.78^{+0.65}_{-0.55}$
u_+ [a]	0.652 ± 0.030	0.668 ± 0.031
u_- [a]	0.098 ± 0.030	0.172 ± 0.031
$h = e \sin\omega$	0.019 ± 0.021	0.006 ± 0.025
$k = e \cos\omega$	-0.016 ± 0.022	0.010 ± 0.031
Orbital eccentricity e	< 0.025	< 0.021
Radial-velocity semi-amplitude K [$\rm m\,s^{-1}$]	375 ± 13	124 ± 5
Systemic velocity $\gamma_{\rm rel}$ [$\rm km\,s^{-1}$]	-37.591 ± 0.007	-35.892 ± 0.004
Derived system parameters		
a/R_*	$6.81^{+0.24}_{-0.20}$	$6.45^{+0.32}_{-0.26}$
$a/R_{\rm p}$	$78.4^{+3.3}_{-2.7}$	$76.4^{+4.8}_{-3.8}$
$(M_\star/{\rm M}_\odot)^{1/3}(R_\star/{\rm R}_\odot)^{-1}$	$0.773^{+0.027}_{-0.022}$	$0.699^{+0.035}_{-0.028}$
Stellar density ρ_* [$g\ cm^{-3}$]	$0.65^{+0.07}_{-0.05}$	$0.48^{+0.07}_{-0.06}$
Impact parameter b	$0.67^{+0.02}_{-0.03}$	$0.70^{+0.03}_{-0.04}$
Atmospheric parameters of the star		
Effective temperature $T_{\rm eff}$[K]	6041 ± 143	5757 ± 134
Surface gravity $\log g$ [cgs] [b]	4.26 ± 0.05	4.15 ± 0.06
Metallicity [Fe/H] [dex]	0.33 ± 0.11	0.26 ± 0.10
Stellar rotational velocity $V \sin i_*$ [$\rm km\,s^{-1}$]	5.5 ± 1.5	4 ± 2
Spectral type	G0V/G0IV	G2IV
Stellar and planetary physical parameters		
Star mass [$\rm M_\odot$] [c]	1.32 ± 0.09	1.19 ± 0.10
Star radius [$\rm R_\odot$] [c]	1.42 ± 0.07	1.52 ± 0.09
Planet mass $M_{\rm p}$ [$\rm M_{Jup}$]	3.23 ± 0.19	1.02 ± 0.07
Planet radius $R_{\rm p}$ [$\rm R_{Jup}$]	1.20 ± 0.06	1.24 ± 0.07
Planet density $\rho_{\rm p}$ [$g\ cm^{-3}$]	2.33 ± 0.36	0.65 ± 0.12
Planet surface gravity $\log g_{\rm p}$ [cgs]	3.75 ± 0.04	3.21 ± 0.05
Stellar rotation period $P_{*,rot}$ [days]	12.9 ± 0.7	
Age of the star t [Gyr]	$2.8^{+1.0}_{-0.8}$	$6.95^{+1.1}_{-1.7}$
Distance of the star d [pc]	1950 ± 250	2250 ± 300
Orbital semi-major axis a [AU]	0.0449 ± 0.0010	0.0455 ± 0.0013
Equilibrium temperature $T_{\rm eq}$ [K] [d]	1637 ± 47	1603 ± 51

a: the non-linear limb-darkening coefficients were fixed for the transit fitting but let vary within their 1-σ error bars during the bootstrap procedure (see text for explanation).
b: from Kepler photometry and evolutionary tracks;
c: from STAREVOL evolutionary tracks;
d: black body equilibrium temperature assuming a uniform heat redistribution to the night-side.

As for KOI-135, only Q1 and Q2 raw light curves were considered. From these curves the flux excess due to contaminating background stars, that is 4.4% and 6.0% for Q1 and Q2 data respectively[7], was subtracted. The KOI-204 light curve, displayed in Fig. 6, shows 35 transits with a period of 3.2 days, a depth of 0.74%, and a duration of 3 hours. Long-term variations with an amplitude of $\sim$ 1% are also seen in the light curve, indicating that the star KOI-204 is a slow rotator. After filtering out such variations, the rms of the light curve is 370 ppm, compatible with the median of the errors of the individual photometric measurements, i.e. 340 ppm.

3.2. Centroid analysis

KOI-204 presents a hint of centroid effect with a shift of 0.72 ± 0.58 mpx in X and 0.66 ± 0.54 mpx in Y (see Fig. 2). According to the MAST database, the main contaminant is the star KIC9305838 with Kepler magnitude $K_{\rm p} = 16.6$, located 8" N from KOI-204. In order to confirm that the transits visible in the Kepler light curve occur on the main target KOI-204, we performed a photometric follow-up of this planetary candidate.

3.3. Ground-based follow-up

3.3.1. Photometric observations

The transit of KOI-204b was observed from the ground during the night of 2011, October the 1st, with a 14-inch telescope at the Oversky Observatory, La Palma. Seventy-four photometric measurements were obtained with a CCD SBIG STL-1001e, using a sloan r' filter and exposure time of 180 s. The angular pixel size is 1.15 arcsec. To keep the observed stars on the same pixel during all the night, we used a tip-tilt SBIG AOL. Photometric

[7] http://archive.stsci.edu/kepler/kepler_fov/search.php

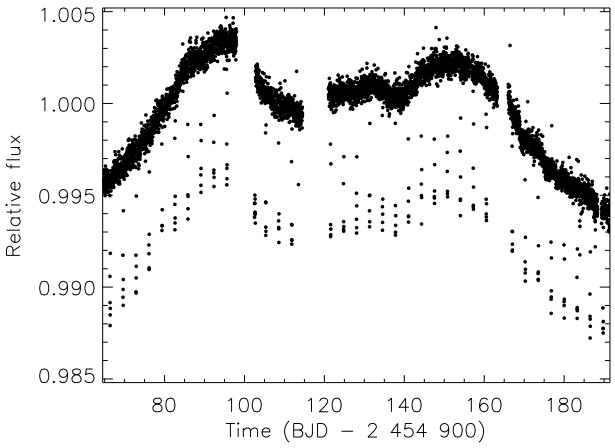

Fig. 6. The Kepler light curve of KOI-204 with a temporal sampling of 29.4 min showing 35 transits and long-term variability.

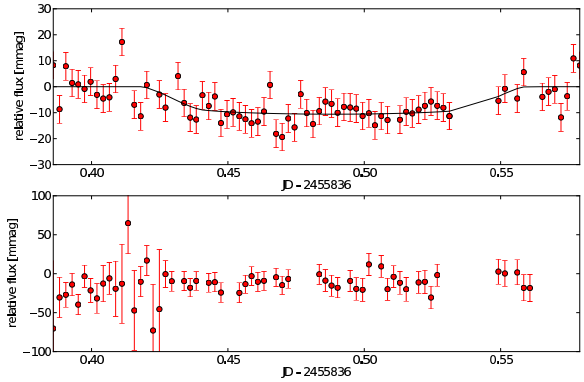

Fig. 7. Ground-based photometric observation of the transit of KOI-204b. *Upper panel*: photometric measurements of the star KOI-204. *Lower panel*: photometric measurements of the main contaminant, the star KIC9305838. The data clearly show that the transit occurs on the target star KOI-204.

observations were reduced using the free software Munipack[8] and are displayed in Fig. 7. They clearly show a transit occurring on the star KOI-204 compatible with those observed by Kepler.

3.3.2. Radial-velocity observations

Seven radial velocities of KOI-204 were secured with the SOPHIE spectrograph. The instrumental mode and measurement extractions were the same as those presented in Sect. 2.3.1. The full width at half maximum of the fitted CCFs is 11.12 ± 0.05 km s^{-1}, and its contrast is 32 ± 3 % of the continuum. Moonlight correction was applied only to one measurement and is relatively modest (20 m s^{-1}).

The radial-velocity measurements are reported in Table 2. The precision ranges between 16 and 46 m s^{-1}. Figure 3 (middle panel) displays them as well as the Keplerian fit from the combined photometry and radial-velocity analysis (Sect. 3.4), assuming a circular orbit as the orbital eccentricity is < 0.021 at 1-σ. This fit gives a reduced χ^2 of 0.6 and is thus acceptable, the standard deviation of the residuals being σ_{O-C} = 9.3 m s^{-1}. The semi-amplitude of the radial-velocity variation is K = 124 ± 5 m s^{-1} (see Fig. 3). No radial-velocity drift was detected over the 13-day span of observation.

Radial velocities measured from cross-correlations with F0, K0, or K5 masks give results similar to those obtained with the G2 mask, and the CCF bisector spans do not show significant variations (Fig. 4, middle panel), so there is no hint for any blend scenario. We can thus conclude that the Kepler photometric signal and spectroscopic observations are due to a hot Jupiter transiting in front of KOI-204. We designate this new planet as KOI-204b.

3.3.3. Stellar characterisation

To derive the atmospheric parameters, the eight SOPHIE spectra, taken to measure the radial-velocity variations, were co-added, after subtracting the background sky light from each spectrum. This allowed us to obtain a single spectrum with a S/N of 25 per pixel (0.02 Å) at 5500 Å. Following the same methodology as described in Sect. 2.3.2, we determined the atmospheric parameters of the host star $T_{\rm eff}$ = 5757 ± 134 K, $\log g$ = 4.59 ± 0.14, and metallicity [Fe/H] = 0.26 ± 0.10. Moreover, no emission was observed in the cores of the Ca II H&K lines, in agreement with the relatively quiescent light curve of KOI-204.

3.4. System parameters

System parameters and their 1-σ errors were derived in the same way as described in Sect. 2.4. They are listed in Table 3. The adopted limb-darkening coefficients for the Kepler bandpass and the spectral type of KOI-204 are $u_{\rm a}$ = 0.448 ± 0.045 and $u_{\rm b}$ = 0.227 ± 0.029 (Sing 2010). Figure 8 shows the phase-folded transit light curve and, overplotted, the transit best fit.

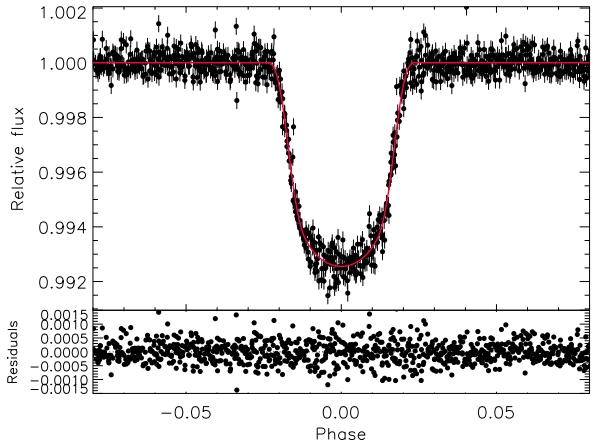

Fig. 8. *Top panel*: Unbinned phase-folded transit light curve of KOI-204. The red solid line shows the transit model rebinned at the Kepler sampling rate (see text for explanation). *Bottom panel*: the residuals from the best-fit model.

3.5. Stellar and planetary parameters

The mass and radius of the parent star, derived from the stellar density given by the transit best fit and STAREVOL evolutionary tracks, are $M_\star$ = 1.19 ± 0.10 M$_\odot$ and $R_\star$ = 1.52 ± 0.09 R$_\odot$. The uncertainties on stellar models were quadratically added to the

[8] http://c-munipack.sourceforge.net

statistical errors on the stellar mass and radius. As for KOI-135, the agreement between the spectroscopic and photometric $\log g$ is at 3-σ level.

According to the aforementioned stellar parameters, KOI-204b has a radius of 1.24 ± 0.07 R_{Jup} and a mass of 1.02 ± 0.07 M_{Jup}, leading to a bulk density of 0.65 ± 0.12 g cm^{-3}. The age of the planetary system is estimated to be $6.95^{+1.1}_{-1.7}$ Gyr.

4. KOI-203 alias Kepler-17

Although fainter than $K_p = 14$, the planetary candidate KOI-203 was followed-up by the Kepler team that, using the High Resolution Spectrometer (HRS) at the Hobby-Eberly Telescope (HET), detected a radial velocity variation of $419.5^{+13.3}_{-15.6}$ m s^{-1}, compatible with a planetary companion (Désert et al. 2011, hereafter D11). This hot Jupiter, renamed Kepler-17b, is interesting as it orbits an active solar-like star in 1.486 day and occults starsposts during transits. Since the stellar rotation period of 11.9 days is almost an integer multiple of the orbital period, the short-cadence Kepler data (Q4-Q6) allowed D11 to see a "stroboscopic" effect: the spots are "mapped" by the planet each 45 ° in longitude. Moreover, since the planet occults the same spots for ∼ 100 days, the true obliquity of the system, i.e. the angle between the stellar rotation axis and the normal to the orbital period, can be estimated close to zero (D11). Last but not least, the high-quality of Kepler data allowed the Kepler team to detect the planetary occultation in the optical with a depth of 58 ± 10 ppm and, consequently, estimate the geometric albedo of Kepler-17b $A_g = 0.10 \pm 0.02$.

We independently followed up this candidate with the SOPHIE spectrograph in spring 2011. With eight new SOPHIE spectra, we are able to refine the orbital and stellar atmospheric parameters and, thus, the characterisation of the planetary system.

4.1. Kepler observations

At the time of starting the radial-velocity follow-up, the public Kepler light curve contained only Q1 and Q2 data with long-cadence rate. Such light curve, corrected from the contamination flux and long-term trends of instrumental origin, is shown in Fig. 9. Stellar variability due to photospheric magnetic activity has a peak-to-peak amplitude of ∼ 3%. The long-cadence data, however, do not allow us to see the occultation of single spots by the planet during the transits, as observed by D11 with short-cadence data (one point per minute).

4.2. Ground-based follow-up

4.2.1. Radial-velocity observations

Eight radial velocities of KOI-203 were secured with the SOPHIE spectrograph in April and May 2011, with the same instrumental mode and measurement extractions as described in Sect. 2.3.1. The full width at half maximum of the fitted CCFs is 10.81 ± 0.12 km s^{-1}, and its contrast is 34 ± 4 % of the continuum. Moonlight correction was applied to all but two measurements, but remains always below 25 m s^{-1}. The radial-velocity measurements are listed in Table 2. Their precision is between 13 and 35 m s^{-1}. Fig. 3 (right panel) displays them as well as the circular Keplerian fit taking the period and transit epoch given by D11. This fit shows an acceptable reduced χ^2 of 1.1 and a

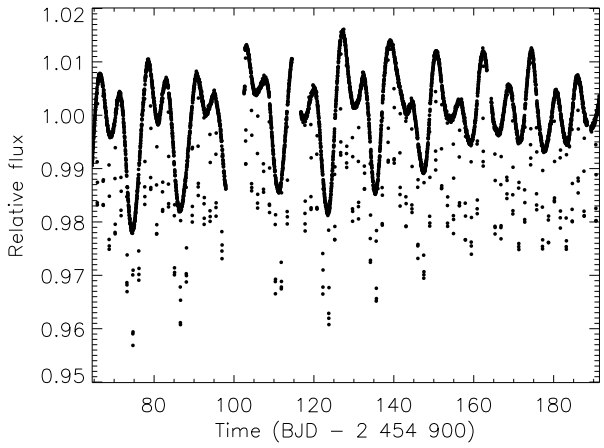

Fig. 9. The light curve of Kepler-17 with a temporal sampling of 29.4 min showing 78 transits and variability with a peak-to-peak amplitude of 3% due to active regions whose visibility is modulated by the stellar rotation.

standard deviation of its residuals $\sigma_{O-C} = 17.8$ m s^{-1}, which indicates that there is no signature of stellar activity in the radial-velocity residuals. The derived semi-amplitude of the radial-velocity variation is $K = 391 \pm 11$ m s^{-1}. Here again, blends scenarios can be excluded as cross-correlations performed with F0, K0, and K5 masks give similar results to those obtained with the G2 mask, and CCF bisector spans are constant (Fig. 4, right panel). We thus concluded in spring 2011 that KOI-203b is actually a transiting hot Jupiter.

Thanks to the radial velocities measured with the HRS spectrograph, D11 derived a slightly less accurate and larger semi-amplitude $K = 419.5^{+13.3}_{-15.6}$ m s^{-1}. Such radial velocities have uncertainties ranging between 26 and 199 m s^{-1}, significantly less precise than those obtained with SOPHIE. The residuals of the HRS Keplerian fit show a 52- m s^{-1} dispersion (D11), to be compared with the 17.8-m s^{-1} dispersion obtained after the best fit of the SOPHIE data.

Our final result is obtained from the combined analysis of the SOPHIE and HRS data (excluding the least accurate HRS measurement) and is, however, mainly driven by the SOPHIE data. We derived $K = 399 \pm 9$ m s^{-1}. No significant radial-velocity drift was detected in the 275-day span of HET and SOPHIE data.

4.2.2. Stellar characterisation

The SOPHIE spectrum, obtained by co-adding the eight individual spectra used for the analysis of radial-velocity variations, was used to derive the atmospheric parameters of the host star Kepler-17. Such a spectrum has S/N= 31 per pixel (0.02 Å) at 5500 Å, higher than the spectrum used by D11, i.e. S/N= 17.5. This allowed us to accurately determine the atmospheric parameters $T_{\rm eff}$, $\log g$, and [Fe/H]. On the contrary, D11 had to fix the $\log g$ to the photometric value due to their low-quality spectrum (see D11, Sect. 3.1, for more details). We found an effective temperature slightly hotter than D11, $T_{\rm eff} = 5781 \pm 85$ K, although compatible at 1.2 σ. The metallicity [Fe/H] and $\log g$ are in good agreement with the values reported in D11: [Fe/H] = 0.26 ± 0.10 and $\log g = 4.53 \pm 0.12$. According to our atmospheric parameters, the B-V of Kepler-17 is 0.66 ± 0.03 (Sekiguchi & Fukugita 2000), significantly lower than 0.82 as estimated by D11. As a

consequence, the activity estimator $\log R'_{HK} = -4.47$ is higher than the value reported by D11, i.e. -4.61.

4.3. Stellar and planetary parameters

The transit fitting was performed in the same manner as for KOI-135b and KOI-204b (see Sect. 2.4) and our transit parameters were in very good agreement with those determined by D11. However, with much more Kepler data and especially short-cadence data, the error bars of D11 are significantly lower than ours, as expected. For that reason, in Table 4 we keep only the transit parameters and related 1-σ errors derived by D11.

From the transit density reported in D11 and STAREVOL evolutionary tracks for the atmospheric parameters of Kepler-17 (Sect. 4.2.2), the stellar mass and radius are estimated to be $M_\star = 1.16 \pm 0.06$ M$_\odot$ and $R_\star = 1.05 \pm 0.03$ R$_\odot$, respectively. From our value of $M_\star$ and the radial-velocity semi-amplitude recomputed with the new SOPHIE measurements (Sect. 4.2.1), by considering a circular orbit and the orbital inclination given by D11, the planet mass is $M_\mathrm{p} = 2.47 \pm 0.10$ M$_\mathrm{Jup}$. The planet radius derived from the stellar radius and the value R_p/R_* reported in D11 is $R_\mathrm{p} = 1.33 \pm 0.04$ R$_\mathrm{Jup}$. All the stellar and planetary parameters are in good agreement with those determined by D11 (always within 1 σ). Our slightly larger stellar mass compensates with the lower radial-velocity semi-amplitude giving almost the same planetary mass as D11.

The most striking difference concerns the age of the planetary system Kepler-17, which, according to our analysis, seems to be younger than 1.8 Gyr (at 1 σ) while D11 found an age of 3.0 ± 1.6 Gyr. The age given by the evolutionary tracks can be compared to that from the gyrochronology since the rotation period has been inferred from the light curve of Kepler-17: 0.9 ± 0.2 Gyr. The "modified gyrochronology" from Lanza (2010) points to an age of 1.7 ± 0.3 Gyr and thus is more consistent with the extreme limit of the age estimated from evolutionary tracks.

4.4. Secondary eclipse and phase variations of KOI-203b

Before the announcement of Kepler-17b by D11, we had independently detected its secondary eclipse and phase variations, although only with Q1 and Q2 Kepler data. This was the main reason why, as for KOI-196b (Santerne et al. 2011), we decided to perform a spectroscopic follow-up of the Kepler planetary candidate KOI-203b.

To detect both the secondary eclipse and phase variations of Kepler-17b, transits were removed from the Q1 and Q2 light curves and the latter were divided in subsets of 4 days, approximately one third of the stellar rotation period. Each subset was then fitted separately with a 4th degree polynomial to remove stellar variability. A 3-σ clipping was applied to this filtered light curve in order to get rid of possible outliers. After performing such a de-trending, the phase variation and secondary eclipse become clearly visible (see Fig. 10). The rms of the light curve filtered by means of a 4th degree polynomial is 260 ppm in relative flux. Using a 3rd degree polynomial gives a worse fit of the stellar variability, giving a larger rms of 350 ppm, while, with a 5th degree polynomial, the rms is equal to 250 ppm and, thus, comparable to that obtained with 4th degree polynomials. This motivates our choice for the use of 4th degree polynomials. In any case, we point out that both the secondary eclipse and phase variations are visible also using 3rd and 5th degree polynomials, although quite barely in the first case because of the significantly increased rms.

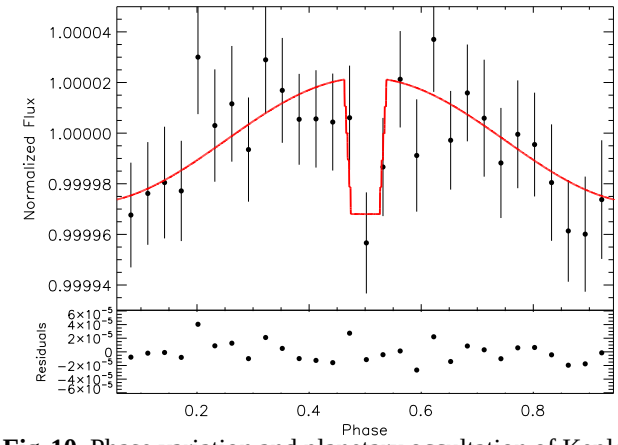

Fig. 10. Phase variation and planetary occultation of Kepler-17b from Q1 and Q2 Kepler photometric measurements. Data were binned in bins of 0.03 in phase.

The phase variations and secondary eclipse were modelled using Eq. 1 in Snellen et al. (2009):

$$F(\phi) = z_\mathrm{lev} \cdot [1 + \sin(\pi\phi)^2 \cdot (1 - F_\mathrm{N/D}) \cdot R_\mathrm{day} + \psi(\phi)] \quad (1)$$

where ϕ is the orbital phase, R_day is the contrast between the planet day-side flux and the stellar flux, i.e. the depth of the secondary eclipse, $F_\mathrm{N/D}$ is the ratio of night-side to day-side flux, and z_lev the stellar brightness. The model of the secondary eclipse $\psi(\phi)$ was computed using the transit model of Giménez (2006) with no limb-darkening and two free parameters: R_day and the time of the secondary eclipse T_sec. The duration of the planetary occultation was fixed to that of the primary transit.

The simultaneous best fit of the phase variations and secondary transit was carried out on the unbinned filtered light curve in the same way as described in Sect. 2.4, i.e. using a Monte Carlo method coupled with the downhill simplex algorithm to search for the global minimum of the χ^2. As for the transit fitting, we oversampled our model (Eq. 1) with a temporal cadence five times denser than the Kepler sampling rate. The error bars of the fitted parameters were estimated with a bootstrap procedure that subtracts the best solution to the data, shifts the residuals in time, adds the subtracted solution and performs again the best fit. Our χ^2 analysis gives $R_\mathrm{day} = 52 \pm 21$ ppm, $F_\mathrm{N/D} = 0$ with an upper limit $F_\mathrm{N/D} < 0.16$ at 1σ, $z_\mathrm{lev} = 0.999973 \pm 0.000011$, and $T_\mathrm{sec} = 2454966.5361 \pm 0.0009$ BJD, corresponding to an occultation phase of 0.5003 ± 0.0006. The best fit is shown in Fig. 10 where we binned the data in bins of 0.03 with the aim of displaying more distinctly the phase variation and the secondary transit. Our value of R_day is perfectly consistent with the occultation depth found by D11, i.e. 58 ± 10 ppm, although our errors are obviously larger as we have only Q1 and Q2 data. The time of the secondary eclipse allows us to constrain $-0.0005 < e\cos\omega < 0.0014$ at 1-σ, where e is the eccentricity and ω the argument of periastron. This is compatible with a circular orbit, as also pointed out by D11. For this reason we had fixed the eccentricity to zero in the analysis of the radial-velocity observations (Sect. 4.2.1).

By using the more precise occultation depth found by D11, and a Kurucz (1993) model spectrum for the star according to the atmospheric parameters given in Sect. 4.2.2, we estimated a brightness temperature $T_\mathrm{d,Kepler} = 2325^{-50}_{+43}$ K in the Kepler bandpass. The planet day-side equilibrium temperature ranges from

Table 4. KOI-203: planet and star parameters.

Fitted system parameters		
Planet orbital period P [days]	1.4857108 ± 0.0000002	Désert et al. (2011)
Planetary transit epoch $T_{\rm tr}$ [BJD-2400000]	$55185.678035^{+0.000023}_{-0.000026}$	Désert et al. (2011)
Planetary transit duration T_{14} [h]	2.276 ± 0.017	Désert et al. (2011)
Radius ratio $R_{\rm p}/R_*$	$0.130307^{+0.00022}_{-0.00018}$	Désert et al. (2011)
Inclination i [deg]	87.22 ± 0.15	Désert et al. (2011)
Quadratic limb darkening coefficient $u_{\rm a}$	0.405 ± 0.007	Désert et al. (2011)
Quadratic limb darkening coefficient $u_{\rm b}$	$0.262^{+0.013}_{-0.015}$	Désert et al. (2011)
Orbital eccentricity e	< 0.001	Désert et al. (2011)
Radial-velocity semi-amplitude K [m s^{-1}]	399 ± 9	This work
Systemic velocity $\gamma_{\rm rel}$ [km s^{-1}]	-24.814 ± 0.007	This work
HET-SOPHIE offset $\gamma_{\rm rel}$ [km s^{-1}]	-0.019 ± 0.014	This work
Derived system parameters		
a/R_*	5.48 ± 0.02	Désert et al. (2011)
$(M_\star/{\rm M}_\odot)^{1/3}(R_\star/{\rm R}_\odot)^{-1}$	1.001 ± 0.020	Désert et al. (2011)
Stellar density ρ_* [$g\ cm^{-3}$]	1.415 ± 0.084	Désert et al. (2011)
Impact parameter b	$0.268^{+0.014}_{-0.012}$	Désert et al. (2011)
Atmospheric parameters of the star		
Effective temperature $T_{\rm eff}$[K]	5781 ± 85	This work
Surface gravity $\log g$ [cgs]	4.53 ± 0.12	This work
Metallicity [Fe/H] [dex]	0.26 ± 0.10	This work
Stellar rotational velocity $V \sin i_*$ [km s^{-1}]	6 ± 2	This work
Spectral type	G2V	
Stellar and planetary physical parameters		
Star mass [${\rm M}_\odot$] [a]	1.16 ± 0.06	This work
Star radius [${\rm R}_\odot$] [a]	1.05 ± 0.03	This work
Photometric surface gravity $\log g$ [cgs]	4.46 ± 0.04	This work
Planet mass $M_{\rm p}$ [${\rm M}_{\rm Jup}$]	2.47 ± 0.10	This work
Planet radius $R_{\rm p}$ [${\rm R}_{\rm Jup}$]	1.33 ± 0.04	This work
Planet density $\rho_{\rm p}$ [$g\ cm^{-3}$]	1.30 ± 0.14	This work
Planet surface gravity $\log g_{\rm p}$ [cgs]	3.54 ± 0.03	This work
Stellar rotation period $P_{*,rot}$ [days]	11.89 ± 0.15	Désert et al. (2011)
Age of the star t [Gyr]	< 1.78	This work
Distance of the star d [pc]	800 ± 100	This work
Orbital semi-major axis a [AU]	0.0268 ± 0.0005	This work
Equilibrium temperature $T_{\rm eq}$ [K] [b]	1746 ± 26	This work
Geometric albedo $A_{\rm g}$	< 0.12	This work

a: from STAREVOL evolutionary tracks;
b: black body equilibrium temperature assuming a uniform heat redistribution to the night-side.

$T_{\rm d} = 1746 \pm 26$ K assuming a uniform heat redistribution to the night side (or, equivalently, a redistribution factor $f = 1/4$ in Eq. 1 of López-Morales & Seager 2007), to 2077 ± 31 K for no redistribution ($f = 1/2$). For the extreme case of a dynamics free atmosphere, where the radiative timescale is shorter than the advective timescale, $T_{\rm d,max} = 2231 \pm 33$ K ($f = 2/3$).

Fig. 11 shows the geometric albedo $A_{\rm g}$ within the 1-σ uncertainty (grey band) as a function of the planet day-side temperature. The dashed vertical lines indicate the values of $T_{\rm d}$ for the aforementioned redistribution factors $f = 1/4, 1/2$ and $2/3$. As usual, $A_{\rm g}$ is estimated by assuming the planet to radiate as a black body and adding a possible reflective component to match the observed occultation depth. However, the planet spectrum can significantly differ from a Planck curve and have a thermal emission in the optical more important than expected from a simple black body (e.g., Fortney et al. 2008; Cowan & Agol 2011 and references therein; see also the discussion by Snellen et al. 2010 about the optical secondary eclipse of CoRoT-2b). Keeping this warning in mind, the geometric albedo, computed as explained above, is comprised between 0.01 and 0.12 (see Fig. 11).

Besides detecting the optical occultation in the Kepler light curve, D11 reported the observations of the Kepler-17b secondary eclipse in the two Spitzer band-passes at 3.6 and 4.5 μm and derived brightness temperatures of $T_{3.6\mu{\rm m}} = 1880 \pm 110$ K and $T_{4.5\mu{\rm m}} = 1770 \pm 150$ K (see D11). If the planet day-side temperature is comprised between the lower and upper limits of the Spitzer brightness temperatures, the geometric albedo would be $0.06 < A_{\rm g} < 0.12$. However, as pointed out by Cowan & Agol (2011), estimating the planet effective temperature with only two Spitzer wavebands can lead to errors on the true value up to 10% (see their Fig. 3). Therefore, $T_{\rm d}$ could be higher than the upper limits given by $T_{3.6\mu{\rm m}}$ and $T_{4.5\mu{\rm m}}$, which would imply an even lower albedo, down to $A_{\rm g} = 0$ if $T_{\rm d} = T_{\rm d,Kepler}$.

The phase variation we detected in the Kepler light curve including only Q1 and Q2 data, tells us that, if all the flux from the planet seen in the optical is thermal in origin, then only a low fraction of stellar heat is transported to the night-side, less than 16% at 1-σ. In this case, the day-side temperature would be close to or higher than ~ 2077 K. We found no evidence for a phase shift in the light curve, which is expected in the case of no

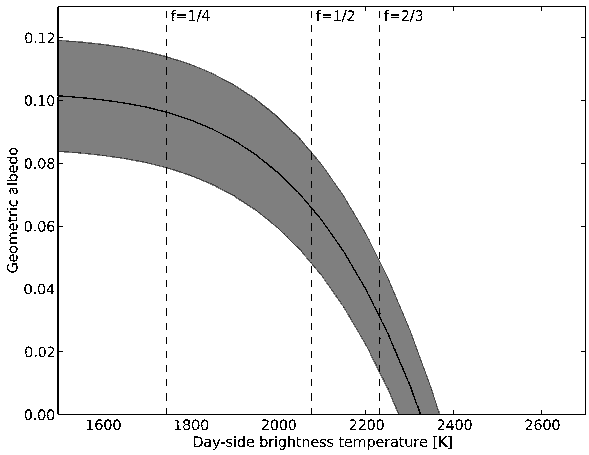

Fig. 11. Geometric albedo as a function of the planet day-side equilibrium temperature. Dashed vertical lines represent the temperature of the planet for i) a perfect heat redistribution to the nightside, $T_{\rm d} = 1746 \pm 26$ K (left), ii) no thermal circulation in the atmosphere, $T_{\rm d} = 2077 \pm 31$ K (middle), and iii) a dynamics free atmosphere where the radiative time scale is shorter than the advective timescale, iii) $T_{\rm d,max} = 2231 \pm 33$ K (right). The grey band covers the albedo values allowed by the 1-σ uncertainty on the occultation depth which is assumed to be the dominant uncertainty.

redistribution, under the assumption that the optical occultation comes entirely from the thermal flux.

As suggested by Cowan & Agol (2011), the observation of the thermal phase variation of Kepler-17b in one of the two IRAC bandpasses, if feasible for such a faint target, would in principle permit to estimate the night-side temperature and, thus, uniquely determine the circulation efficiency, the planet's albedo and its day-side temperature.

Finally, we would like to point out that our recomputed activity estimator $\log R^{'}_{HK} = -4.47$ (Sect. 4.2.2), higher than the value given by D11, reinforces the propensity for a no thermal inversion according to scenario proposed by Knutson et al. (2010) (see also Sect. 7.3 in D11).

5. Summary and conclusions

We reported the discovery of two new hot Jupiters, namely KOI-135b and KOI-204b, and, independently of the Kepler team, confirmed the planetary nature of KOI-203b alias Kepler-17b (Désert et al. 2011), thanks to radial-velocity measurements performed with the SOPHIE spectrograph at the Observatoire de Haute-Provence.

All the three Jupiter-size planets orbit stars with super-solar metallicity, i.e. [Fe/H] ~ 0.3 dex. KOI-135b and KOI-204b have a similar orbital period, $P \sim 3$ days, and radius, $R_{\rm p} \sim 1.2$ $R_{\rm Jup}$, but a different internal structure as their bulk densities differ by a factor of 4, $\rho_{\rm p} = 2.33 \pm 0.36$ and 0.65 ± 0.12 g cm^{-3}, respectively. The density of Kepler-17b lies in between the two, being equal to the Jupiter's one within the error bars. The position of KOI-204b and Kepler-17b in the radius vs mass and mass vs orbital period diagrams of extrasolar planets are fairly common, being two slightly inflated planets. On the contrary, with a mass of 3.23 ± 0.19 $M_{\rm Jup}$, KOI-135b reaches the few known transiting planets with short orbital periods $P < 5$ days and masses between 2.5 and 5 $M_{\rm Jup}$. Those more similar to KOI-135b, in terms of planetary radius and mass, are WASP-32b (Maxted et al. 2011) and HAT-P-16b (Buchhave et al. 2010).

We detected the optical phase variation of Kepler-17b in Q1 and Q2 long-cadence data and showed that the geometric albedo is not well constrained, being $A_g < 0.12$. If all the optical occultation is thermal, then our modelling of the phase variation indicates no redistribution of stellar heat to the night-side with an upper limit of 16% at 1-σ.

Finally, we point out that both Kepler-17 and KOI-135 are interesting targets for a detailed study of their photospheric magnetic activity by means of spot-modelling techniques (e.g., Lanza et al. 2007). The Kepler long-term photometry will permit to derive activity cycles on time-scales of a few years and, more easily, short-term spot cycles as found for CoRoT-2b (Lanza et al. 2009). In principle, this would allow also to search for possible star-planet magnetic interactions.

Acknowledgements. We thank the technical team at the Observatoire de Haute-Provence for their support with the SOPHIE instrument and the 1.93-m telescope and in particular the essential work of the night assistants. We are grateful to the Kepler Team for giving public access to the corrected Kepler light curve and for publishing a list of good planetary candidates to follow-up. Financial support for the SOPHIE observations from the Programme National de Planétologie (PNP) of CNRS/INSU, France is gratefully acknowledged. We also acknowledge support from the French National Research Agency (ANR-08-JCJC-0102-01). A. S. Bonomo acknowledges CNES grant. NCS acknowledges the support by the European Research Council/European Community under the FP7 through Starting Grant agreement number 239953, as well as from Fundação para a Ciência e a Tecnologia (FCT) through program Ciência 2007 funded by FCT/MCTES (Portugal) and POPH/FSE (EC) and in the form of grants reference PTDC/CTE-AST/098528/2008 and PTDC/CTE-AST/098604/2008.

References

Baranne, A., Queloz, D., Mayor, M., et al. 1996, A&AS, 119, 373
Barnes, S. A. 2007 ApJ, 669, 1167
Bathala, N. M., Rowe, J. F., Gilliland, R. L., et al. 2010 ApJ, 713, L103
Borucki, W., J., Koch, D., Basri, G., et al. 2006, In: Planetary Systems and Planets in Systems, Stephane Udry, Willy Benz and Rudolf von Steiger (eds.). ISSI Scientific Reports Series, ESA/ISSI. ISBN 978-92-9221-935-2, 2006, p. 207-220
Borucki, W., J., Koch, D., Basri, G., et al. 2011, ApJ, 736, 19
Bouchy, F., Hébrard, G., Udry, S., et al. 2009, A&A, 505, 853
Bouchy, F., Bonomo, A. S., Santerne, A., et al. 2011, A&A, 553, A83
Buchhave, L. A., Bakos, G., Á., Hartman, J. D., et al. 2010, ApJ, 720, 1118
Casagrande, L., Portinari, L., & Flynn, C. 2006, MNRAS, 373, 13
Cowan, N. B. & Agol, E., 2011, ApJ, 729, 54
Cox, A. N. 2000, Allen's Astrophysical Quantities
Deleuil, M., Bonomo, A. S., Ferraz-Mello, S. et al. 2011, A&A, accepted, arXiv:1109.3203
Désert, J.-M., Charbonneau, D., Demory, B.-O., et al. 2011, submitted to ApJ, arXiv: 1107.5750
Fortney, J.-J., Lodders, K., Marley, M.-S., & Freedman, R. S. 2008, ApJ, 678, 1419
Giménez, A. 2006, A&A, 450, 1231
Giménez, A. 2009, in The Eighth Pacific Rim Conference on Stellar Astrophysics: A Tribute to Kam Ching Leung, Eds. B. Soonthornthum, S. Komonjinda, K.S. Cheng, and K.C. Leung San Francisco: Astronomical Society of the Pacific, Vol. 450, p. 291
Gonzalez, G., 1998, A&A, 334, 221
Hébrard, G., Bouchy, F., Pont, F., et al. 2008, A&A, 481, 52
Jenkins, J. M., Caldwell, D. A., Chandrasekaran, H. et al. 2010, ApJ, 713, L87
Kipping, D. 2010, MNRAS, 408, 1758

Kipping, D., & Bakos, G. 2011, ApJ, 730, 50
Knutson, H. E., Howard, A. W., Isaacson, & H., ApJ, 720, 1569
Kurucz, R. I. 1993, ATLAS9 Stellar Atmosphere Programs and 2 km/s grid. Kurucz CD-ROM No. 13. Cambridge, Mass.: Smithsonian Astrophysical Observatory, 1993.
Lanza, A. F. 2010, A&A, 512, A77
Lanza, A. F. 2009, Pagano, I., Leto, G., et al. A&A, 493, 193
Lanza, A. F., Bonomo, A. S., & Rodonó, M. 2007, A&A, 464, 741
López-Morales, M. & Seager, S. 2007, ApJ, 667, L191
Maxted, P. F. L., Anderson, D. R., Collier Cameron, A., et al. 2011, PASP, 122, 1465
Morton, T. D., & Johnson, A. A. 2011, ApJ, 738, 170
Palacios, A., Calculation of dedicated evolutionary tracks using STAREVOL, private communication.
Pepe, F., Mayor, M., Galland, F., et al. 2002, A&A, 388, 632
Pollacco, D., Skillen, I., Collier Cameron, A., et al. 2007, MNRAS, 385, 1576
Press, W. H., & Rybicki, G. B. 1989, ApJ, 338, 277
Press, W. H., Teukolsky, S. A., Vetterling, W. T., Flannery, B. P. 1992, Numerical recipes in FORTRAN, The art of scientific computing (Cambridge: University Press), 2nd edn
Santerne, A., Díaz, R., Bouchy, F. et al. 2010, A&A, 528, A63
Santerne, A., Bonomo, A. S., Hébrard, G. et al. 2011, A&A, accepted, arXiv:1108.0550
Santos, N. C., Israelian, G., & Mayor, M. 2004, A&A, 415, 1153
Scargle, J. D. 1982, ApJ, 263, 835
Schlegel, D. J., Finkbeiner, D. P., & Davis, M. 1998, ApJ, 500, 525
Sekiguchi, M., & Fukugita, M. 2000, ApJ, 120, 1072
Siess, L. 2006, A&A, 448, 717
Sing, D. K. 2010, A&A, 510, A21
Snellen, I. A. G., de Mooij, E. J. W., & Albrecht, S. 2009, Nature, 459, 543
Snellen, I. A. G., de Mooij, E. J. W., & Burrows, A. 2010, A&A, 513, A76
Sousa, S. G., Santos, N. C., & Mayor, M., et al. 2008, A&A, 487, 373
Sousa, S. G., Santos, N. C., Israelian, G., et al. 2011, A&A, 526, A99
Southworth, J. 2011, MNRAS, in press
Sneden, C. 1973, PhD Thesis, Univ. of Texas